LANGMUIR

pubs.acs.org/Langmuir Article

Ultrathin Atomically Flat Gold Film for Scanning Tunneling Microscopy and Single-Particle Fluorescence Spectroscopy

Zhengyi Bian, Eric Gomez, Jitong Ren, Tathagata Chatterjee, Hao Yang, Charles M. Schroeder, Shuming Nie, Stephan Link,* and Martin Gruebele*

Cite This: *Langmuir* 2025, 41, 16000−16008 Read Online

ACCESS | Metrics & More | Article Recommendations | Supporting Information

ABSTRACT: To enable rear illumination (e.g., TIRF), single-particle fluorescence microscopy, and scanning tunneling microscopy (STM) on the same nanoparticle sample, we investigate the smoothness limit and the thickness limit of template-stripped gold films made with a simple room-temperature deposition protocol ranging from 1 to 200 pm/s on four common substrates: mica, fused silica, silicon, and quartz. The resulting transparent conductive gold film achieves a thickness as low as 9 nm, absorbance as low as 0.2, and a root-mean-square roughness of 80 pm over a 100 × 100 nm^2 area. We further assess whether such gold films enable single-particle characterization by fluorescence imaging and STM imaging on the same sample. Carbon dots, made by a top-down method, with a height as low as 1.0 nm (~3 layers), can be resolved clearly on the gold film island surfaces by using both atomic force microscopy and STM, and the carbon dot single-particle fluorescence blinking can be measured by confocal microscopy. In this way, both optical and electronic characterization can be enabled on the same sample using a substrate that is relatively easy to make in batches.

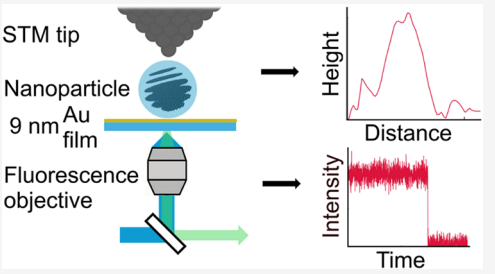

INTRODUCTION

Gold surfaces with atomic smoothness[1] are indispensable substrates for electronic imaging and spectroscopy of nanoparticles, including atomic force microscopy (AFM) and scanning tunneling microscopy (STM). To be suitable substrates for optical imaging techniques such as single-molecule fluorescence, or combined optical-electronic imaging techniques such as single-molecule absorption scanning tunneling microscopy (SMA-STM),[2] gold surfaces must be sufficiently thin to ensure transparency for microscopy access from both sides, while minimizing background fluorescence and maintaining electronic conductivity. Thin films may have reduced collective electron oscillations (surface plasmons) that drive energy dissipation, allowing single-particle optical spectroscopy on the gold film surface. Using these films, it may be possible to characterize single particles, such as carbon dots, using a combination of electronic (e.g., STM) and optical (e.g., confocal fluorescence microscopy) methods.

Despite recent progress, fabricating thin films for combined electronic and optical characterization remains a challenge. Although previous deposition protocols enable fabrication of sufficiently thin (20 nm) conductive transparent gold films with a roughness less than 200 pm,[2−4] these methods often involve high-temperature or variable-temperature deposition, which may not always be available to researchers. Previous protocols also may require metallic (e.g., Pt) matching layers, and have not been tested for the feasibility of single-particle fluorescence detection. Working with subnanoscale materials such as top-down carbon dots (thickness down to ≈1 nm, or three graphene layers) makes stringent demands on substrate quality.[5,6] Ideally, the root-mean-square (RMS) roughness must be maintained below 0.1 nm to preserve high-resolution imaging and a low noise floor. In addition to flatness, optical transmission of ≥ 20% is critical so that excitation beams can penetrate the gold film and enable two-sided optical excitation-detection techniques such as total internal reflection fluorescence (TIRF) microscopy or SMA-STM.[4,7] Thick gold films, while highly conductive and smooth, can excessively quench the fluorescence of nanoparticles due to strong plasmonic and nonradiative interactions.

Here, we adapt a simple room-temperature evaporation and template-stripping protocol[1] to fabricate robust gold films on sapphire substrates suitable for combined optical and electronic characterization of nanomaterials. We refine the protocol as a function of substrate type and deposition rate to identify an optimal set of parameters that produces a surface RMS of ≤80 pm, transmission ≥20%, and maintains high conductivity suitable for STM. Substrates are characterized by using multimodal spectroscopy of top-down synthesized carbon dots on the same sample based on AFM, STM, and

Received: March 4, 2025
Revised: May 21, 2025
Accepted: June 4, 2025
Published: June 17, 2025

https://doi.org/10.1021/acs.langmuir.5c01097
Langmuir 2025, 41, 16000−16008

single-particle fluorescence detected by epifluorescence confocal microscopy.

The optical properties of carbon dots are a topic of debate, with some researchers attributing their high emission yield to small fluorescent molecules rather than to the carbon dots themselves.[5,8−12] For this reason, characterizing carbon dots at the single-particle level by means of multiple techniques like STM and fluorescence microscopy to correlate size and optical properties will help to unravel the mechanism of carbon dot fluorescence.[13,14]

MATERIALS AND METHODS

Materials. Graphite powder (<150 μm, 99.99% trace metals basis, Sigma-Aldrich), N−N-Dimethylformamide (DMF, >99.8%, Fisher Chemical), methanol, dichloromethane, ethyl acetate, sulfuric acid (H_2SO_4), nitric acid (HNO_3), potassium permanganate ($KMnO_4$), potassium persulfate ($K_2S_2O_8$), phosphorus pentoxide (P_2O_5), sodium nitrate ($NaNO_3$), and hydrogen peroxide (H_2O_2) were purchased from Sigma-Aldrich and used as received without further purification. Deionized water was purified using a Milli-Q EQ 7000 Ultrapure Water Purification System to achieve a resistivity of 18.2 MΩ·cm at 25 °C. Dialysis Tubing: Cellulose ester membrane dialysis tubing (MWCO 500−1000 Da) was obtained from Repligen Inc.

High-Grade Muscovite Mica (25 × 25 mm, V1) was purchased from Ted Pella, Inc. Double-sided polished sapphire wafers (C-plane) were sourced from MSE Supplies. P-type B-doped silicon wafers, fused silica wafers, and quartz wafers were obtained from University Wafer Inc. Norland Optical Adhesive (NOA 72) was obtained from Norland Products.

Thin Film Deposition and Stripping. Gold films were prepared based on the template-stripping method with different deposition conditions and substrates, as previously reported.[3] The basic idea is to evaporate gold onto a flat template, clean the exposed back surface of the resulting <15 nm gold film, apply optical epoxy to the back surface of the gold film, apply the final sapphire substrate, cure the optical epoxy, and then gently strip the gold film from the template, so that a thin gold film glued to the sapphire substrate remains. Templates were prepared by dicing fused silica, silicon chips, and quartz chips into 25 × 25 mm^2 shapes from larger wafers using an ADT 7122 Wafer Dicer with an ADT resin blade (00777-8030-005-QKP).

Prior to deposition, all templates except mica were degreased by sonication for 60 min each in acetone, isopropanol (IPA), and methanol, followed by surface cleaning using a Harrick Plasma Cleaner in High Power mode for 30 min per side. When using High-Grade Muscovite Mica V1 (25 × 25 mm^2) as the template, the mica was cleaved immediately before deposition to ensure a pristine surface. Thus, no cleaning process is needed for mica.

Fused silica, silicon, and quartz chips are robust templates that do not readily delaminate and stick to the gold layer when the gold is stripped. However, successfully stripping of an ultrathin gold film (<15 nm) from mica requires careful preparation of the mica to avoid delamination. To ensure a pristine mica surface before Au deposition, mica is cleaved slowly. This approach minimizes fracture of the mica surface and hence steps where the gold film could delaminate during stripping because optical epoxy could penetrate to the mica surface (Figure S1). Additionally, the mica substrate should be sufficiently large (at least 25 × 25 mm^2) to aid in handling. While cleaving with a razor blade to expose a fresh mica surface, some scratching may occur. However, 25 × 25 mm^2 or larger area mica surfaces provide ample usable area for gold film stripping even in the case of a few localized scratches.

Gold films were deposited by electron beam (e-beam) evaporation from >99.999% (Kurt J. Lesker) purity noble metal sources using a Lesker PRO Line PVD 75 evaporator at base pressures of 2.5 × 10^{-6} Torr at room temperature. The deposition rate varied from 1 to 200 pm/s. Fused silica chips, silicon chips, quartz chips, and mica were used as the deposition templates. Average film thickness was determined using a quartz crystal balance. After depositing gold films on the template, and before cementing the final sapphire substrate onto the back surface of the gold film, it was essential to thoroughly clean the gold's back surface because it might be contaminated when exposed in ambient environment. Pressurized air was used to remove dust on the back of the gold film, followed by an oxygen plasma treatment to further remove contaminants from the back surface of the gold film. These steps are essential because contaminants can weaken the integrity and optical quality of the thin gold film. After the cleaning process, UV-curable optical epoxy adhesive was applied to 5 × 8 mm^2 sapphire chips. The gold-coated fused silica, silicon, quartz, or mica was then carefully adhered to the 5 × 8 mm^2 sapphire chips, by gently pressing the sapphire chip with tweezers to remove trapped air bubbles. The adhesive was then cured by exposure under a Traydex 45 UV Curing Machine for 25 min. After curing, the fused silica, silicon, quartz, or mica deposition templates were slowly stripped away, leaving a clean, atomically flat gold film adhered on the sapphire substrate.

UV−Vis Characterization. We cut a fused silica wafer into 12.4 × 40 mm^2 rectangular chips to fit into the holder of the UV−Vis spectrometer, and used the template-stripping method to strip 9, 10, 12, 15, 18, and 20 nm gold films from the mica template onto fused silica. Making sure that the stripped gold film on fused silica covered the entire light path of the UV−Vis spectrometer and keeping the position the same for every measurement, we then collected the UV−Vis absorbance spectrum from 350 to 900 nm.

Synthesis of Graphene Oxide (GO). We used the modified Hummer's method for GO synthesis.[15] The steps are summarized here. We mixed 30 mL concentrated H_2SO_4 (98%), 10 g $K_2S_2O_8$, and 10 g P_2O_5 in a two-necked flask, then stirred the solution over an 80 ± 3 °C oil bath. Adding 8 g of graphite powder to the solution produced a dark mixture stirred at 80 °C for 12 h. We then cooled the mixture naturally to room temperature and added 300 mL DI water slowly (to prevent boiling). We used a paper filter to filter the mixture and wash the pretreated graphite powder with water until the pH was between 5 and 6. The pretreated graphite powder was then dried in a vacuum oven for 8 h at 45 °C.

8 g of the pretreated graphite powder were put into 0 °C precooled concentrated H_2SO_4 (98%, 184 mL). Then we first added 4 g $NaNO_3$, and next 24 g $KMnO_4$ gradually while stirring the mixture at a temperature below 8 °C on an ice bath (caution: make sure the temperature is low enough to prevent explosion). The mixture was stirred over an ice bath for another 2 h. Then it was moved to a 35 °C oil bath and stirred for 12 additional hours. 1500 mL of DI water was added to terminate the reaction. 20 ml of 30% aqueous H_2O_2 was then added and the color changed from brown to yellow. Next, the mixture was filtered by Millipore Stericup Quick Release Vacuum Filtration System with a 0.45 μm pore size PVDF (polyvinylidene fluoride) membrane. 1 N HCl (1000 mL) was used to wash the resulting GO to remove the metal ions. Then 20 L DI water was run though the GO to remove other impurities. We monitored the conductance of the filtrate as an indicator of the effectiveness of the washing: the conductance of the filtrate decreased and stabilized after a few times washing. The GO changed from yellow to brown when using DI water to wash. When the conductance of the filtrate stabilized, the purified GO was freeze-dried.

Synthesis of Top-Down Carbon Dots. Our synthesis is based on the previously reported solvothermal cutting method with modifications in the purification steps.[16] The prepared GO was dispersed in DMF at a concentration of 20 mg/mL and sonicated using a VCX 500 Probe Sonicator (120 W, 100 kHz) for 3 h in an ice bath to prevent overheating. The resulting solution was transferred to a poly(tetrafluoroethylene) (Teflon)-lined autoclave (90 mL) and heated to 200 °C for 8 h. After cooling naturally to room temperature, the product separated into a brown transparent solution and a black precipitate. The black precipitate was first filtered using a paper filter, followed by Whatman Anopore inorganic membrane filters with a pore size of 20 nm. The black precipitate was discarded and the brown filtrate containing the <20 nm diameter carbon dots (or "graphene quantum dots," GQDs) was kept for further processing.

https://doi.org/10.1021/acs.langmuir.5c01097
Langmuir 2025, 41, 16000−16008

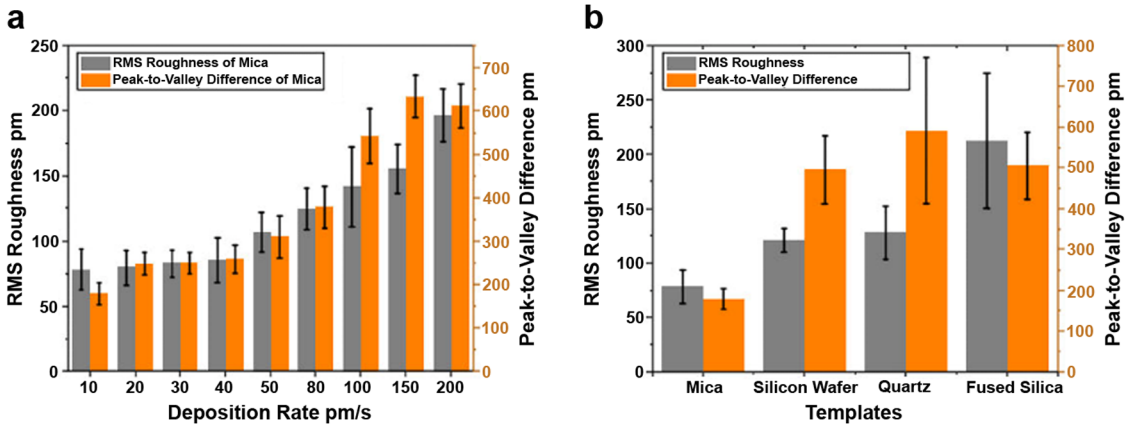

Figure 1. (a) RMS roughness and peak-to-valley difference of template-stripped gold films (15 nm thickness) measured in 100 × 100 nm^2 regions at various deposition rates using mica as the substrate. The error bars represent the variance of RMS roughness and peak-to-valley difference derived from 20 randomly selected 100 × 100 nm^2 areas. (b) Comparative analysis of RMS roughness and peak-to-valley differences for 15 nm stripped gold films deposited at 10 to 200 pm/s on different substrates: mica, silicon wafers, quartz, and fused silica. The error bars represent the variance of RMS roughness and peak-to-valley difference derived from 20 randomly selected 100 × 100 nm^2 areas.

The unpurified carbon dots were obtained by evaporating the DMF using a rotary evaporator. The dried dots were then dispersed in 10 mL of deionized water and dialyzed using cellulose ester membrane tubing (MWCO 500−1000 Da, Repligen Inc.) against 2 L of deionized water for 10 days. During the first 3 days, the buffer was replaced every 6 h and subsequently every 12 h. To prevent rupture due to osmotic pressure, water that diffuses into the tubing was periodically removed. The dialyzed solution was freeze-dried to yield a brown powder.

For further purification, the carbon dots were subjected to silica gel chromatography using a Biotage High-Performance Flash Chromatography (HPFC) System. The sample was loaded on a 100 g Biotage Sfar silica prepacked column. The eluent composition was 1:5 MeOH to EtOAc, and the flow rate was set to 40 mL/min. After collecting the green fractions, the solvent was removed via rotary evaporation, yielding purified carbon dots. The final product was characterized by HR-TEM, single-particle fluorescence imaging, AFM, and STM.

AFM and STM Setups. To test our gold surfaces' suitability for AFM and STM imaging, carbon dots were deposited onto the stripped gold film via aerosol deposition.[13] A solution of 1 μg/mL of carbon dots in ethanol was prepared, and approximately 200 μL of this solution was pulse-sprayed onto the substrate using an Iwata CM-SB airbrush with nitrogen as the carrier gas. The spray distance was maintained at a minimum of 20 cm to ensure even deposition. Following deposition, the sample was placed in a vacuum oven overnight at room temperature to ensure thorough drying.

AFM and STM measurements were performed in air on an Asylum Research Cypher Scanning Probe Microscope. For AFM, a Budget Sensors silicon AFM probe was used in tapping mode, featuring a Tap190Al-G tip with a nominal resonance frequency of 190 kHz and a force constant of 48 N/m. The line scan rate was maintained at 1.95 Hz.

STM measurements were performed with a Bruker 6 mm platinum−iridium tip (80:20 composition), which provide stable and reproducible tunneling conditions. The tunneling currents were set between 50 and 100 pA, with a typical sample bias of 0.2 V, allowing for high-contrast imaging of carbon dots. The STM was carefully calibrated to ensure consistent tip sharpness and stability over prolonged scanning sessions.

Single-Particle Fluorescence Imaging. Single-particle fluorescence imaging was performed on a home-built scanning confocal microscope consisting of an inverted microscope (Zeiss, Axio Observer.D1), a 488 nm diode laser (Coherent, Obis), a 100x (numerical aperture NA = 1.46) oil-immersion objective (Zeiss, α Plan-Apochromat), a piezo scanning stage (Physik Intrumente, P-517.3CL), and an avalanche photodiode (APD) detector (PerkinElmer, SOCM-AQRH-15). A quarter wave plate generated circularly polarized light before excitation. Fluorescence images used for comparison were acquired over an area of 10 × 10 μm consisting of 128 × 128 pixels with an integration time of 1 ms/pixel. A shutter was used to block the excitation beam after the fluorescence image was created. The sample stage was then positioned so that a single fluorescent spot was excited in a confocal geometry, and the emission, filtered by dichroic and long pass filters, was detected by the APD until photobleaching.

Data analysis was performed using an algorithm written in MATLAB 2024a. The user first selects the background of an emission time trace at two points after photobleaching. The trace intensities between these points were averaged and then this averaged background intensity was subtracted from the raw intensity.

RESULTS AND DISCUSSION

The basic idea, as discussed in Methods, is to evaporate gold onto a flat template, clean the exposed back surface of the resulting <15 nm gold film, apply optical epoxy to the back surface of the gold film, apply the final sapphire substrate, cure the epoxy, and then gently strip the gold film from the template, so that a thin gold film glued to the sapphire substrate remains.

We began by fabricating template-stripped gold surfaces for optical and electronic characterization of nanoparticles. Template-stripped gold surfaces are fabricated by first depositing a thin gold film onto a flat template. Although the exposed gold surface is initially rough after deposition, the surface in contact with the template remains flat during and after deposition of gold. Following deposition, the rough exposed surfaces are bonded to a sapphire substrate using optical epoxy. The template is then carefully removed, revealing a nearly atomically flat gold surface. These surfaces are subsequently used for nanoparticle experiments. The roughness of template-stripped gold films mainly depends on the template, deposition rate, and temperature. These factors influence the mobility of gold atoms during deposition,[17,18] which affect the uniformity of the atom distribution, and the interactions between the template and the film, ultimately impacting the surface smoothness. Here, we systematically investigated four readily available substrates: mica, polished fused silica, z-cut quartz, and polished silicon. We scanned the gold deposition rates between 10 and 200 pm/s to determine

https://doi.org/10.1021/acs.langmuir.5c01097
Langmuir 2025, 41, 16000−16008

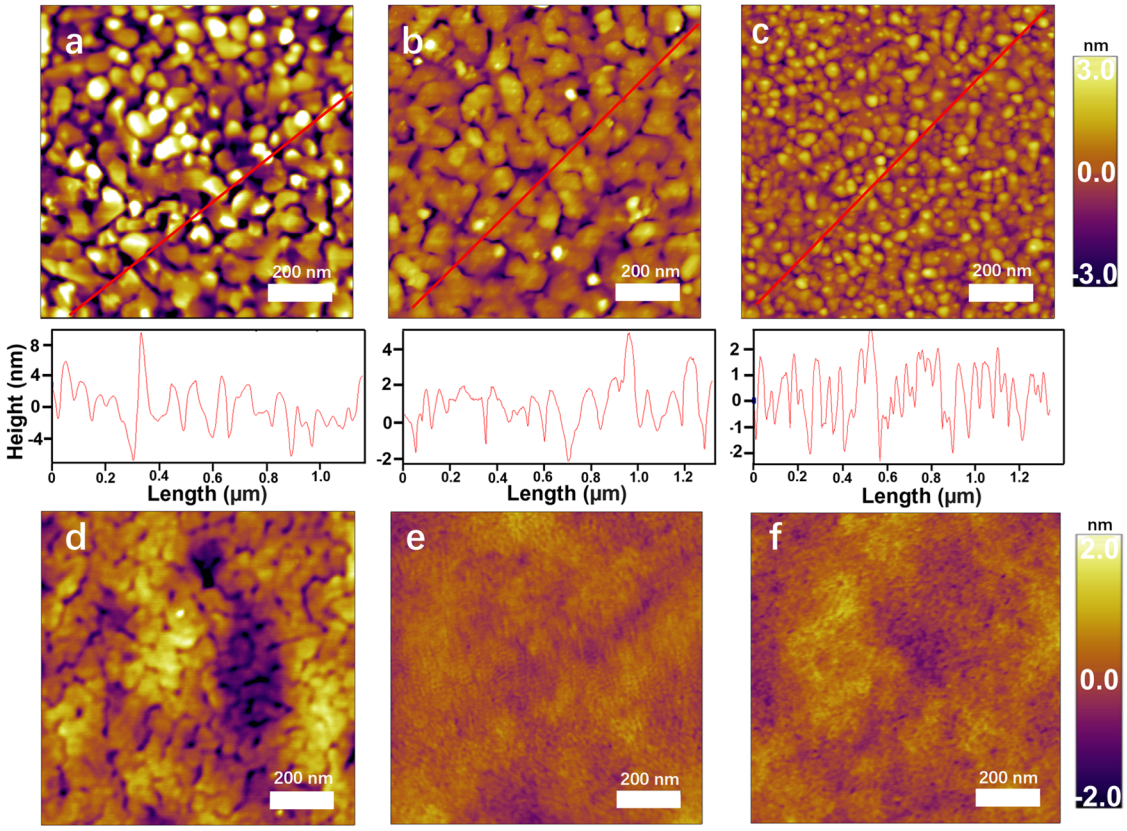

Figure 2. (a–c) AFM images illustrating the surface morphology of the back surface of gold films before stripping, deposited at 1, 10, and 100 pm/s, respectively. The corresponding peak-to-valley differences were around 15, 7, and 6 nm, demonstrating the significant impact of deposition rate on surface smoothness and structural continuity. (d-f) AFM images of template-stripped 15 nm gold films deposited using a combination of 10 nm at 1 pm/s followed by 5 nm at 100 pm/s, a single deposition at 10 pm/s, and a single deposition at 100 pm/s, respectively. These images highlight the ability of combined deposition strategies to balance surface roughness and mechanical integrity. The color bars indicate height variations across the scanned regions.

optimal conditions for producing thin, smooth, and conductive gold films.

In Figure 1a, we illustrate the effect of deposition rate on the resulting template-stripped gold film, using the mica substrate at room temperature (20 °C). Over a 100 × 100 nm^2 area, we see that the average RMS roughness of the gold surface remains similar at about 80 pm, and the average peak-to-valley difference increases slightly from 200 to 250 pm when the deposition rate of gold is increased from 10 pm/s to 40 pm/s. For reference, the diameter of a gold atom is 240 pm. Above that deposition rate the average RMS roughness increases more rapidly from 75 pm at 40 pm/s to over 200 pm at 200 pm/s and the peak-to-valley difference increases to more than 600 pm, or 2 to 3 gold atoms in height. Such roughness would make it difficult to resolve a single carbon dot, which typically consists of a few layers of graphenic carbon with a height as low as 1 nm in both AFM and STM measurements.

Figure 1b compares the best RMS and peak-to-valley roughness for the stripped gold films on all four templates. Mica produced the smoothest films, with polished silicon wafers second best. The Si-templated films typically displayed a slightly higher roughness of about 130 pm RMS, but significantly larger peak-to-valley differences, as well as more pinholes and defects as shown in Figure S4; they were also more time-consuming to fabricate due to extra surface preparation steps, whereas mica required no additional stepsafter cleaving. The inherent imperfections of Si templates could complicate scanning tunneling measurements of ultrasmall structures. Fused silica and z-cut quartz produced rough gold surfaces unsuitable for reliable nanoparticle detection, with RMS roughness on the order of 130 to 220 pm. Although these templates are widely available and easy to handle, our data indicates that they are not as effective as mica or polished silicon wafers for preparing near-atomically flat gold films. For ultrathin stripped gold film, mica is the best out of the four templates when care is taken not to damage the gold film during stripping, and Si could be suitable in automated high throughput applications where robust stripping outweighs the roughly 60% increase in roughness compared to mica. The deposition rate for realizing optimal RMS roughness and peak-to-valley difference in both cases lies between 10 pm/s to 40 pm/s.

We note here that the roughness of the back surface of the unstripped gold film follows the opposite trend with deposition rate as the front surface of the final gold film: the higher the deposition rate, the smoother the back surface. This sets a lower limit on suitable deposition rates to obtain a conductive gold surface. Figure 2a-c compares unstripped gold films deposited on mica at 1, 10, and 100 pm/s, with peak-to-valley differences of approximately 15, 6, and 4 nm, respectively. In particular, the film deposited at 1 pm/s resulted in a discontinuous structure with isolated gold islands; while the island tops are flat enough for imaging, such films are nonconductive and not suitable for STM experiments. Also,

https://doi.org/10.1021/acs.langmuir.5c01097
Langmuir 2025, 41, 16000−16008

stripping such films is generally unsuccessful, likely because discontinuities in the gold film lead to direct contact between the optical adhesive and the mica template during the optical adhesive process, delaminating the mica during the stripping process.

To characterize the surface of 1 pm/s stripped gold, we used a combined deposition strategy: first depositing a 10 nm gold layer at 1 pm/s on mica, followed by a 5 nm adhesion layer at 100 pm/s to ensure continuity (Figure 2d). This approach aimed to fill deep grooves between isolated gold islands, thus preventing contact between the optical adhesive and mica substrate. The combination of a 10 nm layer deposited at 1 pm/s and a 5 nm adhesion layer deposited at 100 pm/s produced films that could be stripped reliably. We found that deposition below 10 pm/s does not improve surface roughness. The peak-to-valley difference is larger than for the stripped films deposited at 10 pm/s and 100 pm/s in a single step based on Figure 2e,f. We assume that the prolonged deposition time at 1 pm/s, requiring approximately 15,000 s for a 15 nm film, can significantly elevate substrate temperature, leading to the formation of islands and deep grooves. For example, as illustrated in Figure S2, depositing 15 nm gold at 10 pm/s at high substrate temperatures (300 °C) resulted in discontinuous, nonconductive films as well. Overall, we conclude that a mica substrate, at room temperature of 20 °C, and a 10 to 40 pm/s deposition rate, while maintaining stable processing conditions throughout the deposition process, is best to fabricate films with optimal smoothness and continuity.

A critical requirement for optical techniques such as SMA-STM and single-particle fluorescence microscopy is achieving sufficient substrate transparency, commonly at least 20% transmittance in the UV−Vis range. This ensures that enough excitation light can reach the nano-objects under study via rear illumination and limits optical heating of the surface, allowing for efficient optical and electronic measurements. The absorbance of the cured thin layer of optical adhesive on the substrate is flat and as low as 0.033 in the range of 350 to 900 nm, corresponding to a transmittance of 93% (uncorrected for reflection), as shown in Figure S3, implying that the substrate is clear and transparent.

We systematically explored gold films ranging from 9 to 20 nm in thickness, all deposited at 10 pm/s on freshly cleaved mica and then stripped with optical adhesive onto a sapphire substrate. We investigated the thickness limit of the gold film to determine the minimum achievable thickness. We deposited 9, 12, 15, 18, and 20 nm gold films on mica because 9 nm is the minimal thickness that can still be reliably peeled off from the mica.

The RMS roughness across four different 100 × 100 nm^2 regions consistently falls within the range of 70−80 pm for all gold films, demonstrating uniform smoothness across the surface. The UV-Vis spectrum of the gold films presented in Figure 3 closely aligns with the theoretical ideal film described in ref 19. Analysis from 350 to 900 nm reveals that thinner films (e.g., 9−12 nm) exhibit higher transmittance in the visible region, as expected. Furthermore, gold films of varying thicknesses display similar absorption spectra within the 350 to 900 nm wavelength range. The overall absorption profile had a characteristic dip near 520 nm and gradually increased toward shorter (350 nm) and longer (900 nm) wavelengths. When reducing the thickness from 20 to 9 nm, the absorption decreased correspondingly. Based on the measured absorbance ($A_{measured}$), we can estimate the transmittance (T) by eq 1.

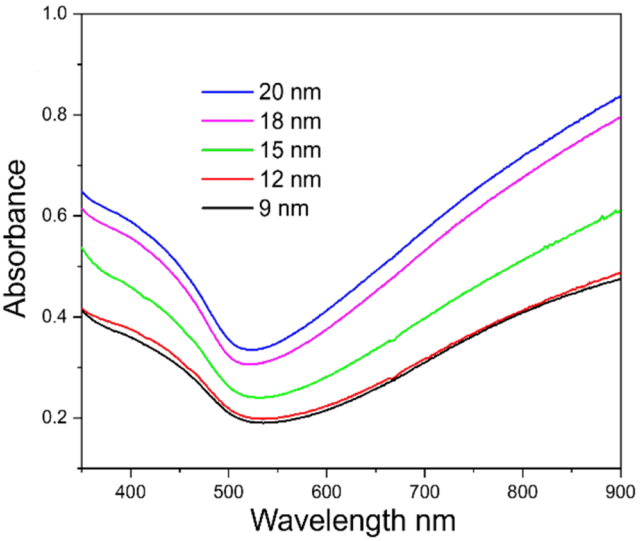

Figure 3. UV−Vis absorbance spectra of template-stripped gold films with thicknesses ranging from 9 to 20 nm in the region between 350 and 900 nm.

$$A_{measured} = -\log_{10}(T) \quad (1)$$

The 9 nm gold film's transmittance increased from 40% at 350 nm to 70% at 520 nm, then decreased gradually to 38% at 900 nm. Even the 20 nm film had a transmittance of 22% at 350 nm, 44% at 520 nm, and 15% at 900 nm. Although the observed decrease with thickness in absorbance deviates from ideal Beer−Lambert behavior, this can be attributed to scattering and reflection at these ultrathin metallic layers. Nevertheless, we found that 9−15 nm films consistently satisfy the ≥20% transmittance criterion over the whole 350−900 nm region, making them suitable for combined optical and scanning probe measurements.

We next tested the stripped gold films for suitability with STM, AFM, and single-particle fluorescence microscopy. 'Top-down' carbon dots are fluorescent nanomaterials made from carbon sources like graphite powder, or carbon nanotubes. Such carbon dots are often disc-shaped, 1−10 nm in diameter and have a height as low as ∼1 nm, or 3 layers of graphene. We deposited the carbon dots from aqueous solution directly onto a 9 nm gold film (10 pm/s, mica template, T = 20 °C processing) by the aerosol gun method and put them in a vacuum oven overnight to remove the solvent. In Figure 4a, the AFM topography of a pristine gold film is shown. The surface is smooth over a 1000 × 1000 nm^2 area, demonstrating minimal roughness and consistent morphology. In a smaller area of 100 × 100 nm^2, the RMS roughness of a typical 100 × 100 nm^2 area is about 80 pm, as seen in Figure 1. The red line in the inset image marks a cross-section selected for height analysis. The corresponding height profile, presented in the graph below panel a, confirms a low peak-to-valley difference, with height variations confined within the range of ±150 pm. The low RMS roughness and peak-to-valley difference indicate a smooth and uniform gold surface.

In contrast, Figure 4b shows the gold substrate after the deposition of carbon dots. The AFM image displays individual carbon dots distributed fairly evenly across the surface, thanks to aerosol deposition. A slight clustering is observable in some

https://doi.org/10.1021/acs.langmuir.5c01097
Langmuir 2025, 41, 16000−16008

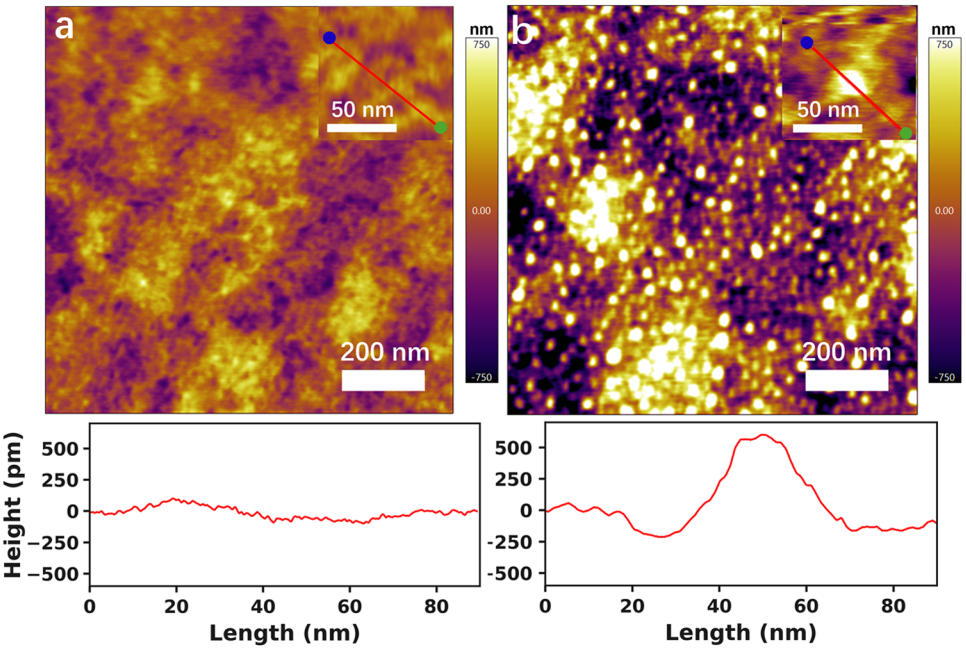

Figure 4. (a) AFM image of a template-stripped 9 nm, 10 pm/s gold film on a sapphire substrate, showcasing its smooth surface over a 1000 × 1000 nm^{2}area. The inset with a 50 nm scale bar shows an area of 100 × 100 nm^2 with a line profile of a selected section, confirming minimal peak-to-valley variations (±150 pm). (b) AFM image of the 9 nm, 10 pm/s gold film after the deposition of carbon dots. Bright features represent individual dots, with measured heights ranging from 1.0 to 1.2 nm (3 to 4 graphenic layers). The inset with a 50 nm scale bar highlights a 100 × 100 nm^2 region with a single dot. These results validate the gold film as a reliable platform for nanoparticle characterization and multimodal analysis.

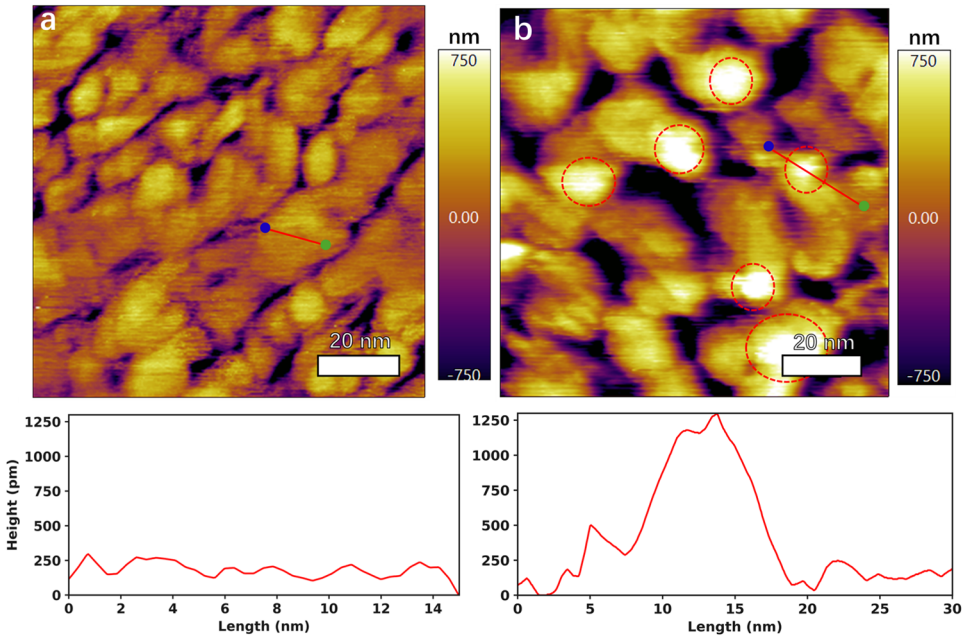

Figure 5. STM characterization of gold films with and without carbon dot deposition. (a) STM topography of a template-stripped 9 nm 10 pm/s gold film on a sapphire substrate, showcasing flat island tops. The corresponding height profile, derived from the red line section, is displayed below. (b) STM topography of a gold film after deposition of carbon dots, marked by the red dashed circles. The height profile of the red line section in panel (b) is shown below.

regions. The observed dots' heights were generally around 1.0−1.6 nm, consistent with the thickness of 3 to 5 graphene layers. The inset provides a higher magnification view (50 nm scale), showcasing that the typical single carbon dot's height is around 1.2 nm. One critical observation is that, despite the presence of these nanofeatures, the underlying gold film maintained its exceptionally smooth baseline roughness, confirming that the template-stripped surface was not disrupted by the nanoparticle deposition and drying steps. Thus, the gold film provides a robust and sufficiently flat platform for accurate single-particle height measurements with processing necessary for deposition.

https://doi.org/10.1021/acs.langmuir.5c01097
Langmuir 2025, 41, 16000−16008

Figure 5 showcases the STM characterization of the same template-stripped gold films, both pristine and after the deposition of carbon dots, along with corresponding height profiles of selected sections. The pristine surface in panel a exhibits relatively smooth and uniform morphology, typical of our template-stripped gold substrates. The surface features display nanoscale roughness, with the red line marking a section selected for detailed height analysis. The corresponding height profile is presented in the graph below panel a, consistent with the roughness described earlier. Panel b shows the STM topography of a gold film after deposition of carbon dots. The surface morphology reveals distinct protrusions marked by red dashed circles, suggesting the successful adsorption of carbon dots onto the gold surface. The numbers of the carbon dots in 100 × 100 nm^2 of both AFM and STM images are comparable in magnitude, within experimental variation. The red line in the STM image highlights a specific section used for height analysis, and shows an electronic height of 1.0 ± 0.1 nm above the baseline of the gold surface. For the six dots circled in Figure 5b, the measured electronic height varies from 1 to 1.6 nm.

The 9 nm gold film's resistance across the film is ≈25 Ω, which is measured by placing two multimeter tips. Complementary STM measurements on a 90-day-aged substrate (Figure S5) reveal that the gold film remains flat and suitable for deposition, as shown in Figure S5a, and highly conductive, as evidenced by the linear I−V curve collected on the bare film in Figure S5b. The tunneling resistance of the gold film is ≈2 GΩ. A carbon dot trace recorded on an individual carbon dot (Figure S5c) confirms that both the substrate integrity and dot conductivity are preserved after prolonged ambient exposure and the carbon dot's I−V curve reveals a typical semiconductor's I-V curve.

Gold films are optically flat and do not show significant autofluorescence, enabling weakly fluorescing molecules or particles, such as carbon dots, to show emission when deposited on the atomically flat thin gold layer. 10 μm × 10 μm fluorescence images of the gold film were obtained by scanning the sample over a focused 488 nm laser beam in a home-built confocal microscope setup. Figure 6a shows a clean gold surface with low emission background, although a few weakly fluorescent regions are visible due to surface contamination when exposed to atmosphere or fluorescent defects on the surface.

Under the same imaging conditions, fluorescence images of carbon dots deposited on the gold layer exhibited significantly higher fluorescence counts, as shown in Figure 6b. The optical transparency and atomically thin dimensions of the gold layer are sufficient to prevent quenching the emission of carbon dots. The high density of carbon dots distributed on the gold film, similar to that seen in AFM images in Figure 4, is prominent as indicated by the elevated counts relative to the background.

As reported previously for our specific carbon dots, the carbon dot emission is mainly from the surface chromophores, as determined by conducting surface modification experiments (e.g. pH tuning, and surface modification).[20] To confirm the nature of the carbon dot fluorescence, emission intensity as a function of time was recorded for representative particles (labeled I and II in Figure 6b). These temporal trajectories display single-step bleaching (Figure 6c,d), characteristic of the single chromophoric behavior of top-down carbon dots. The decay at the tail end of the bleaching in Figure 6d results from

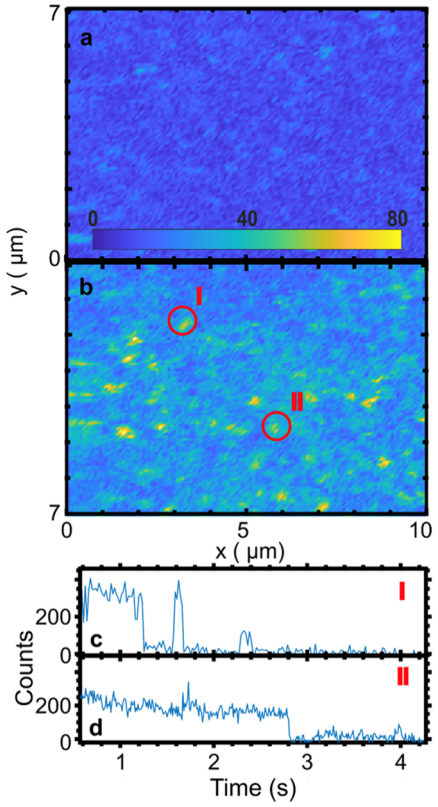

Figure 6. (a) An optically clean gold film exhibits only weak background emission. The scanned 70 μm^2 fluorescence image of the bare gold film without carbon dots excited with 13 kW/cm^2 at 488 nm. (b) About a dozen high-density carbon dots are visible on the aerosol-deposited surface and easily distinguished from background emission. The scanned 70 μm^2 fluorescence image of carbon dots deposited on the gold film is also excited with 13 kW/cm^2 at 488 nm. (c) Intensity trajectory of bright spot I in panel (b). Single-step bleaching to the background distinguishes fluorescent from gold film emission. (d) Same as (c) for spot II in panel (b).

the contributions of other nearby carbon dots in the dense sample, collectively producing a prolonged emission profile.

Hence, by combining the optical transparency necessary for laser-based excitation with the atomic-scale smoothness required for high-resolution STM, these template-stripped ultrathin gold films facilitate multimodal interrogation of nanoparticles on the same substrate.

■ CONCLUSIONS

We have successfully developed an atomically flat, partially transparent, and highly conductive gold film, optimized at a deposition rate of 10−40 pm/s at room temperature (20 °C) on mica substrates. This deposition rate was found to strike an ideal balance between achieving minimal surface roughness and maintaining the mechanical integrity of the film, outperforming both lower rates (e.g., 1 pm/s), which led to isolated islands and higher rates (e.g., 100 pm/s), which increased surface roughness and peak-to-valley differences. These films demonstrate exceptional surface smoothness, with RMS roughness values as low as 80 pm and peak-to-valley differences of 200 ± 50 pm, while maintaining mechanical integrity and conductivity even at a minimum thickness of 9 nm. The films offer ≥20% transparency in the UV-Vis range depending on thickness, which is critical for SMA-STM and

https://doi.org/10.1021/acs.langmuir.5c01097
Langmuir 2025, 41, 16000−16008

fluorescence-based studies of nanoscale systems. The ultrathin gold films enable single-particle characterization of nanoscale materials, with correlative multimodal studies combining STM, AFM, and optical measurements on the same substrate. Additionally, we validated the surface coverage and distribution of carbon dots by correlating particle counts from both STM and AFM measurements, confirming the consistency and reliability of these multimodal imaging techniques on the same substrate. The ability to resolve subnanoscale features, coupled with high optical transmittance and electrical conductivity, highlights the unique versatility of these films. Furthermore, the fabrication process,using a simple template-stripping method and readily available materials, ensures scalability and reproducibility, making these films suitable for widespread applications.

■ ASSOCIATED CONTENT

Supporting Information

The Supporting Information is available free of charge at https://pubs.acs.org/doi/10.1021/acs.langmuir.5c01097.

The SI file discusses the stripping process of the gold film on fractured and smooth templated mica, AFM characterization of the gold film at higher temperature, the optical transmission of cured adhesive on sapphire, AFM characterization of a 15 nm gold film on silicon at room temperature, and STM characterization (I-V curves) of gold films with carbon dots deposited on them. (PDF)

■ AUTHOR INFORMATION

Corresponding Authors

Stephan Link − *Department of Chemistry and Department of Electrical and Computer Engineering, University of Illinois Urbana−Champaign, Urbana, Illinois 61801, United States;* orcid.org/0000-0002-4781-930X; Email: slink@illinois.edu

Martin Gruebele − *Department of Chemistry, Beckman Institute for Advanced Science and Technology, Center for Biophysics and Quantitative Biology, Department of Physics, and Carle-Illinois College of Medicine, University of Illinois Urbana−Champaign, Urbana, Illinois 61801, United States;* orcid.org/0000-0001-9291-8123; Email: mgruebel@illinois.edu

Authors

Zhengyi Bian − *Department of Chemistry and Materials Research Laboratory, University of Illinois Urbana−Champaign, Urbana, Illinois 61801, United States*

Eric Gomez − *Department of Chemistry, University of Illinois Urbana−Champaign, Urbana, Illinois 61801, United States;* orcid.org/0000-0002-9017-1836

Jitong Ren − *Department of Chemical and Biomolecular Engineering and Beckman Institute for Advanced Science and Technology, University of Illinois Urbana−Champaign, Urbana, Illinois 61801, United States*

Tathagata Chatterjee − *Department of Chemistry, University of Illinois Urbana−Champaign, Urbana, Illinois 61801, United States;* orcid.org/0009-0002-0427-559X

Hao Yang − *Beckman Institute for Advanced Science and Technology and Department of Materials Science and Engineering, University of Illinois Urbana−Champaign, Urbana, Illinois 61801, United States*

Charles M. Schroeder − *Department of Chemical and Biomolecular Engineering, Beckman Institute for Advanced Science and Technology, Department of Materials Science and Engineering, and Center for Biophysics and Quantitative Biology, University of Illinois Urbana−Champaign, Urbana, Illinois 61801, United States;* orcid.org/0000-0001-6023-2274

Shuming Nie − *Department of Chemistry, Beckman Institute for Advanced Science and Technology, Department of Bioengineering, and Department of Electrical and Computer Engineering, University of Illinois Urbana−Champaign, Urbana, Illinois 61801, United States;* orcid.org/0000-0002-7328-1144

Complete contact information is available at: https://pubs.acs.org/10.1021/acs.langmuir.5c01097

Author Contributions

Z.B., E.G., J.R., T.C., and H.Y. performed research. Z.B., E.G., and M.G. analyzed data. M.G. and Z.B. designed the research and wrote the manuscript. C.M.S., S.N., S.L., and M.G. supervised research. All authors edited the manuscript. All authors have given approval to the final version of the manuscript.

Funding

This work was supported by a CCI grant from the National Science Foundation (CHE-2124983), under the Center for Adopting Flaws as Features. E.G. acknowledges support from the NSF Graduate Research Fellowship Program (DGE 21-46756).

Notes

The authors declare no competing financial interest.

■ ACKNOWLEDGMENTS

Z.B. extends gratitude to Dr. Tucson Richelson (Holonyak Micro & Nanotechnology Lab) and Dr. Pengcheng Sun (Illinois Materials Research Laboratory) for their guidance and assistance with the e-beam evaporator. Additional thanks go to Dr. Kathy Walsh (Illinois Materials Research Laboratory) for her training and support with AFM and STM, as well as to Dr. Ziwen Wang and the Nie Lab for their help in wet-lab management and safety protocols. Z.B. also appreciates the insightful advice provided by Dr. Christy Landes.

■ REFERENCES

(1) Putnam, A.; Blackford, B. L.; Jericho, M. H.; Watanabe, M. O. Surface Topography Study of Gold Deposited on Mica Using Scanning Tunneling Microscopy: Effect of Mica Temperature. *Surf. Sci.* **1989**, *217* (1−2), 276−288.

(2) Carmichael, E. S.; Gruebele, M. Controlling the Smoothness of Optically Transparent Gold Films by Temperature Tuning. *J. Phys. Chem. C* **2009**, *113* (11), 4495−4501.

(3) Wagner, P.; Hegner, M.; Guentherodt, H.-J.; Semenza, G. Formation and in Situ Modification of Monolayers Chemisorbed on Ultraflat Template-Stripped Gold Surfaces. *Langmuir* **1995**, *11* (10), 3867−3875.

(4) Nienhaus, L.; Scott, G. E.; Haasch, R. T.; Wieghold, S.; Lyding, J. W.; Gruebele, M. Transparent Metal Films for Detection of Single-Molecule Optical Absorption by Scanning Tunneling Microscopy. *J. Phys. Chem. C* **2014**, *118* (24), 13196−13202.

(5) Bian, Z.; Wallum, A.; Mehmood, A.; Gomez, E.; Wang, Z.; Pandit, S.; Nie, S.; Link, S.; Levine, B. G.; Gruebele, M. Properties of Carbon Dots versus Small Molecules from "Bottom-up" Synthesis. *ACS Nano* **2023**, *17* (22), 22788−22799.

(6) Nguyen, H. A.; Srivastava, I.; Pan, D.; Gruebele, M. Unraveling the Fluorescence Mechanism of Carbon Dots with *Sub* -Single-Particle Resolution. *ACS Nano* **2020**, *14* (5), 6127−6137.
(7) Nienhaus, L.; Goings, J. J.; Nguyen, D.; Wieghold, S.; Lyding, J. W.; Li, X.; Gruebele, M. Imaging Excited Orbitals of Quantum Dots: Experiment and Electronic Structure Theory. *J. Am. Chem. Soc.* **2015**, *137* (46), 14743−14750.
(8) Essner, J. B.; Kist, J. A.; Polo-Parada, L.; Baker, G. A. Artifacts and Errors Associated with the Ubiquitous Presence of Fluorescent Impurities in Carbon Nanodots. *Chem. Mater.* **2018**, *30* (6), 1878−1887.
(9) Yuan, L.; Yan, M.; Tao, X.; Yang, X.; Long, W.; Xia, W.; Liao, H.; Gong, Y.; Zhang, K.; Xia, Z.; Fu, Q. Efficient Synthesis of High-Purity Carbon Dots via Self-Polymerization Driven Bottom-up Growth for High-Selectivity Sensing and High-Efficiency Separation. *Carbon* **2024**, *226*, No. 119169.
(10) Righetto, M.; Privitera, A.; Fortunati, I.; Mosconi, D.; Zerbetto, M.; Curri, M. L.; Corricelli, M.; Moretto, A.; Agnoli, S.; Franco, L.; Bozio, R.; Ferrante, C. Spectroscopic Insights into Carbon Dot Systems. *J. Phys. Chem. Lett.* **2017**, *8* (10), 2236−2242.
(11) Righetto, M.; Carraro, F.; Privitera, A.; Marafon, G.; Moretto, A.; Ferrante, C. The Elusive Nature of Carbon Nanodot Fluorescence: An Unconventional Perspective. *J. Phys. Chem. C* **2020**, *124* (40), 22314−22320.
(12) Bian, Z.; Gomez, E.; Gruebele, M.; Levine, B. G.; Link, S.; Mehmood, A.; Nie, S. Bottom-up Carbon Dots: Purification, Single-Particle Dynamics, and Electronic Structure. *Chem. Sci.* **2025**, *16*, 4195.
(13) Nguyen, H. A.; Srivastava, I.; Pan, D.; Gruebele, M. Ultrafast Nanometric Imaging of Energy Flow within and between Single Carbon Dots. *Proc. Natl. Acad. Sci. U.S.A.* **2021**, *118* (11), No. e2023083118.
(14) Gomez, E.; Mehmood, A.; Bian, Z.; Lee, S. A.; Tauzin, L. J.; Adhikari, S.; Gruebele, M.; Levine, B. G.; Link, S. Single-Particle Correlated Imaging Reveals Multiple Chromophores in Carbon Dot Fluorescence. *J. Am. Chem. Soc.* **2025**, *147*, No. jacs.5c01367.
(15) Xu, Y.; Bai, H.; Lu, G.; Li, C.; Shi, G. Flexible Graphene Films via the Filtration of Water-Soluble Noncovalent Functionalized Graphene Sheets. *J. Am. Chem. Soc.* **2008**, *130* (18), 5856−5857.
(16) Zhu, S.; Zhang, J.; Liu, X.; Li, B.; Wang, X.; Tang, S.; Meng, Q.; Li, Y.; Shi, C.; Hu, R.; Yang, B. Graphene Quantum Dots with Controllable Surface Oxidation, Tunable Fluorescence and up-Conversion Emission. *RSC Adv.* **2012**, *2* (7), 2717.
(17) Hegner, M.; Wagner, P.; Semenza, G. Ultralarge Atomically Flat Template-Stripped Au Surfaces for Scanning Probe Microscopy. *Surf. Sci.* **1993**, *291* (1), 39−46.
(18) Priest, C. I.; Jacobs, K.; Ralston, J. Novel Approach to the Formation of Smooth Gold Surfaces. *Langmuir* **2002**, *18* (6), 2438−2440.
(19) Kossoy, A.; Merk, V.; Simakov, D.; Leosson, K.; Kéna-Cohen, S.; Maier, S. A. Optical and Structural Properties of Ultra-Thin Gold Films. *Adv. Opt. Mater.* **2015**, *3* (1), 71−77.
(20) Zhu, S.; Zhang, J.; Tang, S.; Qiao, C.; Wang, L.; Wang, H.; Liu, X.; Li, B.; Li, Y.; Yu, W.; Wang, X.; Sun, H.; Yang, B. Surface Chemistry Routes to Modulate the Photoluminescence of Graphene Quantum Dots: From Fluorescence Mechanism to Up-Conversion Bioimaging Applications. *Adv. Funct. Mater.* **2012**, *22* (22), 4732−4740.

https://doi.org/10.1021/acs.langmuir.5c01097
Langmuir 2025, 41, 16000−16008